C. R. Physique 14 (2013) 619–628

Contents lists available at SciVerse ScienceDirect

Comptes Rendus Physique

www.sciencedirect.com

Trends and perspectives in solid-state wetting / Mouillage solide–solide : tendances et perspectives

Solid-state wetting on nanopatterned substrates

Mouillage à l'état solide sur les substrats nano-patternés

Yukio Saito [a,*], Maxime Ignacio [b], Olivier Pierre-Louis [b]

[a] *Department of Physics, Keio University, Yokohama 223-8522, Japan*
[b] *Institut Lumière Matière, UMR 5306, Université Lyon-1–CNRS, Université de Lyon, 69622 Villeurbanne cedex, France*

ARTICLE INFO

Article history:
Available online 31 July 2013

Keywords:
Cassie–Baxter state
Wenzel state
Nanogrooves
Nanopillars

Mots-clés :
État de Cassie–Baxter
État de Wenzel
Nanotranchées
Nanopiliers

ABSTRACT

We review some recent results on the morphology of heteroepitaxial overlayers deposited on nanopatterned substrate surfaces. We mainly focus on modeling based on kinetic Monte Carlo (KMC) simulations. On arrays of parallel grooves or arrays of pillars, we find three main classes of states similar to those known for liquids: (i) Cassie–Baxter states, where solid islands sit on top of the substrate structure; (ii) Wenzel states, where solid islands are in contact with the bottom of the substrate; and (iii) solid imbibition (also denoted as capillary filling for parallel grooves), where the solid forms a film in the substrate surface structure. This multi-stability is controlled by the wettability parameter χ, and shape transitions exhibit hysteresis. We discuss the dynamics of the collapse of a Cassie–Baxter to Wenzel state, and the collapse of the Wenzel state to an imbibition film. We also discuss the possibility to grow crystals in the CB state on nanopatterned substrates. During growth, the crystals formed in CB state merge, leading to a continuous polycrystalline overlayer where the size of the grains is controlled by the distance between pillars.

RÉSUMÉ

Nous résumons quelques résultats récents sur la morphologie de couches hététoépitaxiées sur des substrats patternés. Nous nous focalisons sur la modélisation par simulations Monte Carlo cinétique. Sur des réseaux de tranchées parallèles, nous trouvons trois états principaux analogues à ceux connus pour les liquides : (i) les états de Cassie–Baxter, dans lesques les îlots solides restent au sommet des structures du substrat ; (ii) les états de Wenzel, dans lesquels les îlots sont en contact avec le fond des structures ; (iii) les états d'imbibition, où le solide forme un film dans la structure de la surface du substrat. Cette multistabilité est controlée par le paramètre de mouillabilité χ, et les transitions de forme présentent de l'hystérésis. Nous discutons la dynamique de collapse de l'état de Cassie–Baxter vers l'état de Wenzel, et de ce dernier vers l'état d'imbibition. Pendant la croissance, les cristaux formés dans l'état de Cassie–Baxter se rejoignent pour former une surcouche continue, dont la taille des grains est contrôlée par la distance entre les piliers.

* Corresponding author.
E-mail addresses: yukio@rk.phys.keio.ac.jp (Y. Saito), maxime.ignacio@univ-lyon1.fr (M. Ignacio), olivier.pierre-louis@univ-lyon1.fr (O. Pierre-Louis).

1631-0705/$ – see front matter
http://dx.doi.org/10.1016/j.crhy.2013.06.010

1. Introduction

Heteroepitaxy is a useful technique to grow a crystalline film that cannot solidify spontaneously, such as gallium nitride (GaN) crystals on (0001) sapphire substrates. One merit of using a single crystal substrate is the possible control of the crystal orientation due to the lattice structure, but there are some demerits because adsorbate molecules differ from substrate molecules. This has two main consequences: (i) the adsorbate–adsorbate and adsorbate–substrate interaction energies are different, and (ii) there is usually a mismatch between the adsorbate and the substrate lattice parameters. Because of these effects, the adsorbate layer may dewet on the substrate, or cracks may appear. For example, the lattice mismatch in heteroepitaxial growth of a GaN layer on sapphire substrate is as large as $\sim$ 13.8%, and the epilayer contains many cracks when GaN is deposited directly on sapphire [1].

However, using the deposition of a low-temperature buffer layer before growing the thick GaN epilayer, single crystal films with optically flat surfaces free from cracks were grown [1]. Since buffer layers are grown at low temperatures, crystallites in the buffer layer are found to exhibit a columnar structure [2]. During subsequent deposition of GaN at a high temperature a GaN nuclei is nucleated on top of each column of a fine buffer crystalline pillar. After geometrical selection only grains that grow the fastest are expected to survive [2]. Since the area of direct contact between sapphire substrate and the buffer crystallite is small, misfit strain is easily relaxed at side edges of buffer crystallites. Thus, further deposition of the GaN layer is less affected by strain.

Another example of heteroepitaxy on patterned substrates is GaN deposition on Si nanopillar arrays [3]. The deposited adsorbate is found to stay mainly on top of the pillars with voids underneath between substrate pillars. Thus, the adsorbate does not wet the substrate. In this dewetting overlayer the dislocation density is observed to be reduced as compared to the case without substrate patterning. Similar dewetting phenomenon is observed in the liquid film on a flat or patterned substrate [4]. In both liquid and solid cases adsorbate films may be in Cassie–Baxter (CB) states with voids underneath the adsorbate [5,4], in Wenzel (W) states where the gap between pillars is filled by adsorbate [6,4], and in imbibition states where the adsorbate forms a film within the substrate structure. On the other hand, there are important differences between liquid and solid wetting: mass transport is controlled by hydrodynamics for liquids, whereas it is controlled by surface diffusion for solids; surface tension is isotropic for liquids while it is anisotropic for crystalline solids; in addition, misfit strain is present in solids but not in liquids. In the past five years, we have been studying wetting or dewetting statics and dynamics for solid adsorbates on nanopatterned substrates by means of kinetic Monte Carlo (KMC) simulations [7–11]. In the following, we review some results of these works.

First, the KMC model is introduced in Section 2. Then, the steady-states of an island on parallel nanogrooves are discussed in Section 3. We find three possible states: CB, W and capillary filling (CF). In Section 4, we discuss the statics and the dynamics of shape transitions of islands on nanopillars. Finally in Section 5, the growth dynamics of crystalline layers on nanopillars are simulated in order to study the possibility to achieve a CB state. The whole study is summarized and future directions are discussed in Section 6.

2. Lattice-gas model

Solid-on-solid (SOS) models [12,13] are often used for the analysis of wetting/dewetting phenomena of heteroepitaxial adsorbate films on a flat substrate [14–17]. However, since they do not allow void formation underneath solid adsorbate layers, SOS models are inappropriate here. Then, the simplest extension of the SOS model is a 3D lattice-gas model, where space is divided into lattice sites, and each site is occupied by an adsorbate atom A or by a substrate atom S or it can be empty.

Substrate atoms are assumed to exhibit strong mutual interaction so that the substrate remains frozen. Adatoms are assumed to move on the surface of the adsorbate or of the substrate. For an adatom on the surface to move, it has to break chemical bonds formed with neighboring atoms. The interaction strength of the nearest neighbor (NN) pair of adatoms is J_1[1] and the one of the next nearest neighbor (NNN) pair is J_2. Their ratio

$$\zeta = \frac{J_2}{J_1} \tag{1}$$

determines the equilibrium crystal shape (ECS). Without NNN interactions, i.e. when $\zeta = 0$, the ECS at $T = 0$ is a cube enclosed only by (100) facets. With a finite ζ, the (110) and (111) facets appear in the ECS, as shown in Fig. 1(a). The extension of each facet is determined by the surface free energy at a finite temperature T. At low temperatures, the roughness of the facets is very small. Therefore, the surface free energies per unit area can be approximated by the surface energy per unit area of a perfectly flat facet. These expressions can be obtained using a bond counting method. For example, a (100) facet atom exhibits one nearest neighbor and 4 next nearest neighbor broken bonds leading to an energy cost $(1/2)(J_1 + 4J_2)$ per facet atom. Since the area occupied by one atom is a^2, one finds $\epsilon_{100} = (J_1 + 4J_2)/(2a^2)$. Using a similar calculation for the (110) and (111) facets one finds

[1] We here use generically the letter J for interaction energies in our lattice-gas models, which corresponds to an exchange interaction of Ising spins with $S_z = \pm 1/2$ [13]. Note that there is a factor of 4 difference in J when choosing $S_z = \pm 1$.

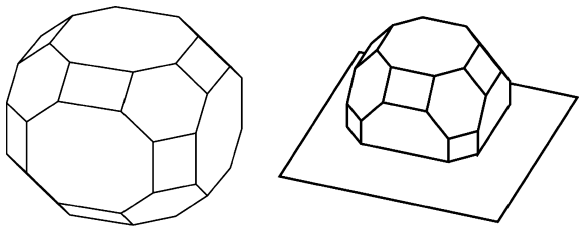

Fig. 1. Equilibrium crystal shape with NN and NNN interactions [18]. (a) Isolated and (b) on substrate.

$$\epsilon_{1jk} = \frac{J_1}{2a^2}(1+j+k)^{1/2}\left[1+(4-j-k)\zeta\right] \tag{2}$$

where j, k are equal to 0 or 1. Here a is the lattice parameter of a simple cubic crystal. The (100) facet exhibits an octagonal shape, the (111) has a hexagonal shape, and the (110) has a rectangular shape, as shown in Fig. 1(a).

Adatoms also interact with NN and NNN substrate atoms with interaction strengths J_{s1} and J_{s2}, respectively. Their ratio is simply set to the same value as between adatom pairs $J_{s2}/J_{s1} = \zeta$ in order to reduce the number of free parameters. On the other hand, the ratio of an adatom interaction with a substrate atom J_{s1} to that with an adatom J_1 defines a new parameter,

$$\chi = \frac{J_{s1}}{J_1} \tag{3}$$

hereafter denoted as the wettability, which controls the wetting of an adsorbate island on the substrate. On a flat substrate an adsorbate layer completely wets the substrate when $\chi \geqslant 1$, whereas for $\chi \leqslant 0$ it completely dewets the flat substrate. For an intermediate value, $0 < \chi < 1$, an adsorbate island partially wets the substrate, as shown in Fig. 1(b).

The surface energy per unit area for (001) orientation is given by Eq. (2): $\epsilon_{\mathrm{AV}}(001) = (J_1 + 4J_2)/2a^2$. Assuming that we break the substrate–adsorbate interface into two free surfaces, we obtain the relation $\epsilon_{\mathrm{SA}}(001) = \epsilon_{\mathrm{SV}}(001) + \epsilon_{\mathrm{AV}}(001) - (J_{s1} + 4J_{s2})/a^2$, where $\epsilon_{\mathrm{SV}}(001)$ is the substrate surface energy per unit area. As a consequence:

$$\chi = \frac{1}{2}\left(1 + \frac{\epsilon_{\mathrm{SV}} - \epsilon_{\mathrm{SA}}}{\epsilon_{\mathrm{AV}}}\right) \tag{4}$$

For a liquid droplet on a solid surface, surface and interface free energies per area are isotropic, and the contact angle θ satisfies the Young relation:

$$\gamma_{\mathrm{SV}} - \gamma_{\mathrm{SA}} = \gamma_{\mathrm{AV}} \cos\theta \tag{5}$$

By replacing surface free energies per area γ of liquid by solid surface energies per area ϵ at the zero temperature, the wetting parameter χ of Eq. (4) is related to the liquid contact angle θ as:

$$\chi = \frac{1}{2}(1 + \cos\theta) \tag{6}$$

This relation allows one to link the energy balance described by the parameter χ, and the local geometry in the vicinity of the triple line described by the contact angle θ. It is possible to extend the definition of the contact angle to the case of anisotropic surfaces as long as the surface is not faceted. In the presence of a faceted adsorbate surface at the triple line, the contact angle is fixed by the facet orientation. In this case, the contact angle does not vary when varying χ over a finite range. Therefore, under these circumstances there is no one-to-one correspondence between θ and χ. The reason behind this is that θ describes the local shape of the island close to the triple line, while facets are extended (non-local) features on the equilibrium shape. In order to describe the macroscopic shape of the island globally rather than the vicinity of the triple line, we here define the order parameter for wetting as the ratio of the area $\mathcal{N}_{\mathrm{AV}}$ of the adsorbate surface to that $\mathcal{N}_{\mathrm{SA}}$ of the adsorbate–substrate interface:

$$\psi = \frac{\mathcal{N}_{\mathrm{AV}}}{\mathcal{N}_{\mathrm{SA}}} \tag{7}$$

For an isotropic island, the ECS is a spherical cap with a contact angle $\theta = \cos^{-1}(2\chi - 1)$, and the order parameter is $\psi = 1/\chi$. For an adsorbate island with rectangular parallelepipedic shape with a square cross section of width L and height h, the volume is $V = L^2 h$. By minimizing surface energy, the width is determined as $L = V^{1/3}/(1-\chi)^{1/3}$ with a height $h = (1-\chi)L$, and the order parameter is $\psi = 5 - 4\chi$.

In order to study the statics and dynamics of an adsorbate island on patterned substrates, kinetic Monte Carlo (KMC) simulations were performed. Therein, adatoms diffuse along the adsorbate island surface or on the substrate surface. For an adatom surrounded by n_i neighboring atoms where i represents the type of bonds, $i = 1, 2, s1$ and $s2$, the rate of its jump to one of the NN sites at a temperature T is written as $\nu = \nu_0 \exp[-\sum_i n_i J_i / k_{\mathrm{B}} T]$, where ν_0 is an attempt frequency.

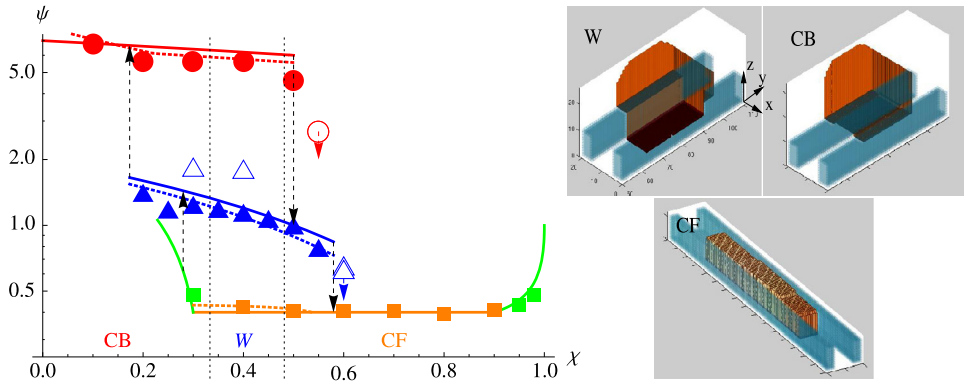

Fig. 2. From [7]. KMC simulations and analytical model, with $k_BT/J_1 = 0.5$, $\zeta = 0.2$, $\lambda = 20a$, and $N = 10^4$. Vertical dotted lines separate different ground states (indicated close to the axis). Left panel: two-loop hysteresis diagram of the wetting parameter ψ. Solid line: model with (100) facets only. Dotted lines: model with all facets. Open symbols indicate non-equilibrated runs. The two points above the W state are obtained with a different initial condition. The green branches correspond to states that exist only due to finite-size effects. In the limit of large islands $v \to 0$ (i.e. $N \gg (\lambda/a)^3$), finite-size effects disappear and the green branches vanish. The right panel shows typical configurations for the three states in KMC simulations. The island is in red, and the substrate is in light-blue. Color available online.

3. Statics on parallel nanogrooves

The simplest pattern on a substrate surface is a one-dimensional array of nanogrooves. We studied the shape variations of the adsorbate island on a substrate with nanogrooves as a function of the wettability parameter χ [7]. The system exhibits multi-stability, and several states are observed, as shown in Fig. 2. When the wetting parameter χ is small, an adsorbed island stays on top of the grooves. This is the Cassie–Baxter (CB) state. Upon increasing χ, an island extends its bottom in the groove gap, and the bottom touches the base of the groove, leading to the Wenzel (W) state. For a large value of the wetting parameter χ, an island fills the capillary between grooves, and we call it the capillary filling (CF) state. (Note that the CF state enters into the more general class of solid imbibition discussed below in more details for substrates with pillar arrays.)

We now describe the system in more details. In an array of parallel grooves with a periodicity λ, each groove is set to have a square cross section with the same depth and width $\lambda/2$. On this nanopatterned substrate, an adsorbate island in a rectangular parallelepiped shape with a width λ, a height h and a length ℓ is provided initially, and the shape relaxation is simulated by the KMC method. During the surface diffusion of adatoms, the total number of adatoms is kept fixed as $N = \lambda h \ell / a^3$. The wetting order parameter ψ of islands in steady-state varies as a function of the wettability parameter χ, as shown in Fig. 2 for $\zeta = 0.2$. Insets indicate corresponding island shapes.

For small χ, the island stays on top of the grooves and the CB state is stable. The value of the order parameter depicted by circles in Fig. 2 agrees with the theoretical expectation evaluated by energy minimization at $\zeta = 0$:

$$\psi_{\mathrm{CB}} = 7 - 2\chi \tag{8}$$

At $\chi = 0.5$, the bottom of the island starts to extend in the groove, and the island collapses to the W state. Decreasing the wettability χ, the island remains in the W state for a while, and it returns to the CB state only at a very small value of χ around $\chi \approx 0.2$: the island shape shows hysteresis. The order parameter ψ depicted by triangles agrees with the theoretical estimation for the W state:

$$\psi_{\mathrm{W}} = 2 - 2\chi \tag{9}$$

Increasing the wettability χ, the W state collapses to a CF state at $\chi \approx 0.6$. Up to $\chi = 0.9$, the island fills the groove capillary with an island top being at the same level as the top of the groove. The order parameter depicted by squares agrees well with the theoretically estimated constant value for the CF state,

$$\psi_{\mathrm{CF}} = \frac{1}{3} + \frac{1}{12v} \tag{10}$$

where $v = Na^3/\lambda^3$ is the relative volume. For large wettability $\chi > 0.9$, the island flattens by lowering its top height less than the groove top. At $\chi = 1$, the adsorbate completely wets the substrate such that the adsorbate monolayer covers the substrate. Decreasing χ, the adsorbate island in the CF state starts to increase its height to the W state around $\chi = 0.3$.

Even with the simplification that $\zeta = 0$, leading to islands with (100) facets only, the theoretical estimates given in Eqs. (8), (9) and (10) fit well with simulation results, as drawn in Fig. 2, since the NNN interaction is set as small as $\zeta = 0.2$. With this calculation, the minimum energy configuration is determined. The CB state is the state with the lowest energy for $\chi \leqslant \chi_{\mathrm{CB|W}}$, the W state for $\chi_{\mathrm{CB|W}} \leqslant \chi \leqslant \chi_{\mathrm{W|CF}}$, and the CF state for $\chi \geqslant \chi_{\mathrm{W|CF}}$, where:

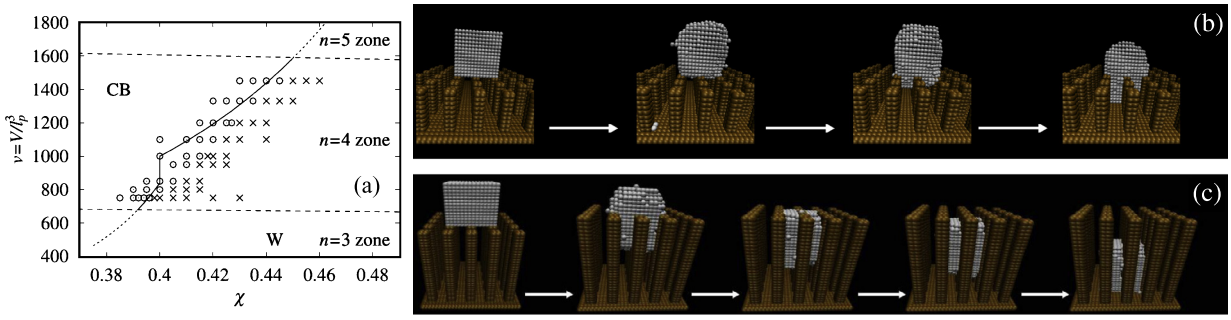

Fig. 3. (a) From [8]. Phase diagram of an adsorbate island on an array of pillars in the phase space of an island volume $V = vl_p^3$ and wettability χ. Circles represent the points where the island stays on top of pillars (CB state), whereas crosses indicate that the islands collapse down to the W state. (b) KMC simulation of the collapse to a Wenzel state, starting from an initial condition where the island is in an unstable Cassie–Baxter state. (c) From [11]. KMC simulation of collapse on high pillars. The irreversible impalement is followed by a vertical diffusion along the pillars, which ends when the island touches the bottom of the substrate. Color available online.

$$\chi_{\mathrm{CB|W}} = \frac{1}{3} \quad \text{and} \quad \chi_{\mathrm{W|CF}} = \frac{2}{3} - \frac{5 + 4\sqrt{6v+1}}{72v} \tag{11}$$

However, multiple states coexist for a given χ, and metastable states can coexist with the most stable state. Metastable states cannot relax to the equilibrium state due to the presence of an energy barrier much larger than the thermal energy $k_B T$. The upper and the lower limits of metastability are evaluated from the disappearance of the energy barriers. The threshold values of the wettability $\chi_{\mathrm{A}\to\mathrm{B}}$ for the transitions from state A to state B are theoretically estimated as [7]:

$$\begin{aligned}
&\chi_{\mathrm{CB}\to\mathrm{W}} = 1/2 \\
&\chi_{\mathrm{W}\to\mathrm{CB}} = 1/3 - (1+\sqrt{1+30v})/36v \\
&\chi_{\mathrm{W}\to\mathrm{CF}} = 2/3 - (1+\sqrt{1+6v})/36v \\
&\chi_{\mathrm{CF}\downarrow} = 1 - 1/8v \\
&\chi_{\mathrm{CF}\uparrow} = 1/3 - 1/24v
\end{aligned} \tag{12}$$

where we have defined the transitions $\chi_{\mathrm{CF}\downarrow}$ and $\chi_{\mathrm{CF}\uparrow}$ at which the CF state height becomes lower or higher than the groove height, leading to the branches in green in Fig. 2. Note that these branches exist only due to finite-size effects, and disappear as $v \to \infty$ [7]. The predictions of Eq. (12) are in good agreement with simulation results, as shown in Fig. 2.

4. Statics and dynamics on nanopillars

4.1. Statics of CB stability

As discussed above, an island on substrate grooves takes various states as a function of wettability parameter. However, there is up to now no corresponding experiment to our knowledge. Instead, there are experiments of adsorbate crystals on a substrate with nanopillars [3]. Therefore, we now study an island on an array of nanopillars [8]. Pillars have a square cross section of area ℓ_p^2 and a height h_p. They are arranged in a square pattern with a periodicity ℓ_x. The initial shape of an adsorbate island is a cube on the top of $n \times n$ pillars. The stable state of an island depends on the island volume V and the wettability parameter χ. For a large island or with a small wettability χ, the island stays on top of pillars in the CB state. In contrast, for a small island or with a large wettability χ, the island collapses down to the W state. A part of the phase diagram is shown in Fig. 3.

A closer look indicates three possible configurations in the CB state on $n \times n$ pillars. When the island is small, the outer edge of the island stays inside pillar tops, which we call the inner state. As the volume increases, the outer edges of an island reach the pillar edges, and are pinned. Thus, the island width stops increasing and only the island height increases. This state is called the pinned state. Only after the island shape becomes a cube with the volume $[(n-1)\ell_x + \ell_p]^3$, the island width starts to increase. The edges of an island extend beyond pillar tops, and this state of a cubic island is called an outer state.

As the wettability χ increases, the CB state is shown to collapse to the W state. In the range of parameter under consideration, close to the transition boundary, the state with the lowest energy is always the W state. The CB state is either metastable or unstable. For example, during the transition from the inner state of the CB configuration to the W state, the island bottom starts to extend down to wet pillar walls, as depicted in Fig. 4(a). The energy variation from the CB state ΔE is calculated at various island volumes $v = V/\ell_p^3$ as a function of the extension h^* of the island bottom. For a large island with $v = 750$, there is a finite energy barrier, but for a small island with $v = 720$ the energy barrier disappears, indicating the instability of the CB state, as shown in Fig. 4(b). The theoretically obtained stability limit at $T = 0$ is drawn

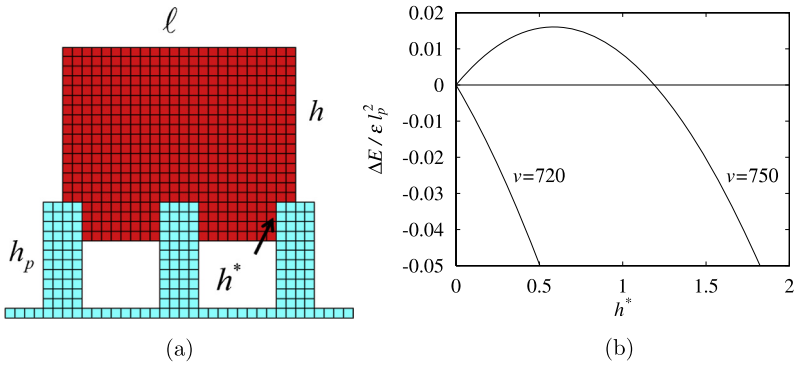

Fig. 4. From [8]. Energy barrier for the collapse from the CB to the W states. (a) Side view of the collapsing process from the inner CB state. (b) Excess energy ΔE as a function of the down elongation h^* of the island bottom. A large island with a volume $v = 750$ has a finite energy barrier, whereas a small island with $v = 720$ loses the barrier for $\chi = 0.395$. Color available online.

by straight lines in the phase diagram, Fig. 3(a). Because of these three different shapes for the CB state (inner, pinned and outer), the theoretical stability limit consists of three segments. It agrees fairly well with simulation results at a finite temperature.

4.2. Dynamics: instability of the CB state

The dynamics of the collapse of an island from an unstable CB state is shown in Fig. 3. Once again, the expression of various quantities can be obtained in the limit $\zeta \to 0$, and are found to be in good agreement with KMC simulations at $\zeta = 0.2$. We start with an island of height h_0 and lateral extent $\ell = (n-1)\ell_x + \ell_p$ in the pinned state. The total time of irreversible collapse to the Wenzel state reads [11]:

$$\mathcal{T}_W = \frac{h_p \ell (1-\phi^2)}{16 \Omega D_{ad} \Delta C} \left[h_p \left(\frac{1}{1-\phi} - 1 + \phi^2 \right) + 2h_0 \right] \tag{13}$$

where h_p is the pillar height, $\phi = n\ell_p/\ell$, D_{ad} is the adatom diffusion constant, and $\Delta C = C_{eq}(\exp[\mu_*/k_B T] - \exp[\mu/k_B T])$, with C_{eq} the equilibrium adatom concentration on the island surface. In addition, the chemical potentials at the top and bottom facets are defined as $\mu = 4\gamma_{AV}\Omega/\ell$, and $\mu_* = \mu[1-\phi+(n-1)(1-2\chi)\phi]/(1-\phi^2)$, where Ω is the atomic area. We expect that formulas similar to Eq. (13) apply to the inner and outer states.

When the pillars are high enough, the island does not reach the bottom of the pillars during irreversible impalement. The island is impaled up to the configuration where the pillar tops reach the island top. The time of irreversible impalement from the pinned state is then [11]:

$$\mathcal{T}_c = \frac{h_0^2 \ell}{16 \Omega D_{ad} \Delta C} \left(1 + \frac{1}{(1-\phi)^2 (1+\phi)} \right) \tag{14}$$

Then, since there is still a gap under the island, the island starts to diffuse along the pillars. The island diffusion process stops when the island reaches the bottom of the substrate after a time [11]:

$$\mathcal{T}_d = \frac{(h_p - h_i)^2}{2D_i} \tag{15}$$

where D_i is the island diffusion constant, and $h_i = h_0/(1-\phi^2)$ where h_i is the height of an island (along z) when it is completely impaled. When χ is small enough, the island diffusion is limited by adatom surface diffusion and $D_i \sim 1/N$ where N is the number of atoms in the island. However, the situation is more complex for large χ. Indeed, KMC simulations indicate that D_i oscillates with N, suggesting that the equilibrium shape itself may oscillate with N, as found in the experiments of Ref. [19]. In the minimum of the oscillations, the island diffusion constant is limited by two-dimensional nucleation of top and bottom facets [11]. Note that when χ is large, the diffusion process is more complex due to the interaction of the island with the top of the pillars [11].

4.3. Dynamics of solid imbibition

When χ is large, the W state is unstable and the solid adsorbate penetrates the gap between pillars. Imbibition is characterized by the formation of a film which has the same height as the pillars. This can be seen as the opposite of the Cassie–Baxter state, which is characterized by the formation of a void film under the island. This phenomenon shares similarity with the imbibition of liquids in micropatterns [20], and we call it solid imbibition. We consider pillars of height

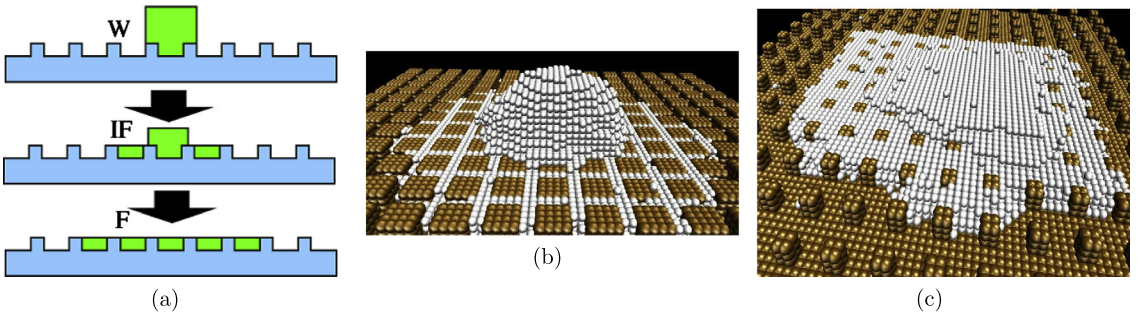

Fig. 5. From [10]. Solid imbibition. (a) Transition from the W state via the island-and-film (IF) state to the film (F) state. (b) Imbibition with narrow channels, and (c) with wide channels. Color available online.

h_p and a square cross section of width ℓ_p are arranged periodically both in the x and y directions with the periodicity ℓ_x. Imbibition is found to occur for χ larger than:

$$\chi_\mathrm{imb} = 1 - \frac{2h\ell_\mathrm{p}}{\ell_x^2 + 4h\ell_\mathrm{p} - \ell_\mathrm{p}^2} \tag{16}$$

For $\chi_\mathrm{imb} < \chi < 1$, an adsorbate island initially prepared in a W state spreads in the substrate structure. During the imbibition dynamics, an island stays on top of the imbibition film, as shown in Fig. 5(a). We name this state the island-and-film (IF) state. Eventually, the top island disappears and only the film remains, which we call the film (F) state, as schematically represented by Fig. 5(a).

Depending on the gap width $\ell_x - \ell_\mathrm{p}$ between pillars, two modes of island spreading are observed. When the gap between pillars is narrow, the adsorbate spread smoothly to form a circular imbibition film, as shown in Fig. 5(b). The spreading area increases roughly linearly in time, or the wetting front moves in proportion to square-root of time. The driving force for imbibition in this case is the chemical potential difference between the island and the film edges, and adatoms diffuse from the top of the film to the film edge. A quantitative description of the imbibition dynamics can be achieved assuming that the limiting process is adatom diffusion [10].

When the gap between pillars is wide, on the other hand, the wetting front is square in shape reflecting the pillar arrangement as shown in Fig. 5(c). The imbibition front is pinned by pillars. The front motion is now governed by nucleation events as in Fig. 5(c). Indeed, thermal fluctuations induce excursions of the front. Once these excursions reach the next row of pillars, they grow irreversibly laterally, and the whole front moves from one row of pillars to the next. The energy barrier for the nucleation estimated theoretically agrees qualitatively with the simulation results obtained from the statistical analysis of the incubation time of nucleation in KMC simulations [10].

5. Deposition growth on patterned substrate

So far we mainly discussed steady-states and the shape transition dynamics of islands on a patterned substrate. We now wish to discuss the formation of adsorbate islands on nanopatterned substrates during growth by deposition. More precisely, we wish to understand the conditions under which islands can be formed in the CB state during growth, despite the fact that the W state has a lower energy, or even when the CB state is unstable.

When deposition is so slow that a small island has sufficient time to relax, the adsorbate layer ends up in the W state since it has a lower energy. In fact, when water drops are grown on a nanopatterned superhydrophobic substrate, a few large drops grow in the Wenzel state [21] or a mixed state with Wenzel and filled channel [22]. However, in experiments of heteroepitaxial crystal growth of GaN on Si nanopillars [3], deposited adsorbate stays mainly on top of nanopillars, and empty space is allowed beneath the adsorbate solid.

In order to analyze the possibility of growth in the Cassie–Baxter state, we discuss models which have little or no island relaxation dynamics, and which are appropriate when the growth rate is fast enough (or the temperature low enough), so that the processes discussed in the previous sections (collapse, imbibition, etc.) can be neglected.

A typical model of crystal growth under deposition which allows vacancies and overhangs is the ballistic deposition (BD) model [23]. In the BD model, adatoms are deposited normally onto the flat substrate, and when they touch another adatom or a substrate atom, they freeze immediately on the spot. In the BD model, the grown adsorbate forms an irregular solid aggregate, as shown in Fig. 6(a), and the growth front is known to be self-affine. For a BD model on a one-dimensional substrate of a lateral size L, the growth front is defined by the highest height $h(i)$ of a column i for $1 \leqslant i \leqslant L$. The average front height is defined by $h = L^{-1}\sum_{i=1}^{L} h(i)$, and the front width by $\mathcal{W} = (L^{-1}\sum_{i=1}^{L}[h(i) - h]^2)^{1/2}$. The self-affine feature of the growth front is specified by scaling relations such that $\mathcal{W}$ increases in proportion to h^β for low h, and $\mathcal{W}$ saturates to the value proportional to L^α for high enough h. Here, α is the roughness exponent and β is the growth exponent. The scaling relation takes the form

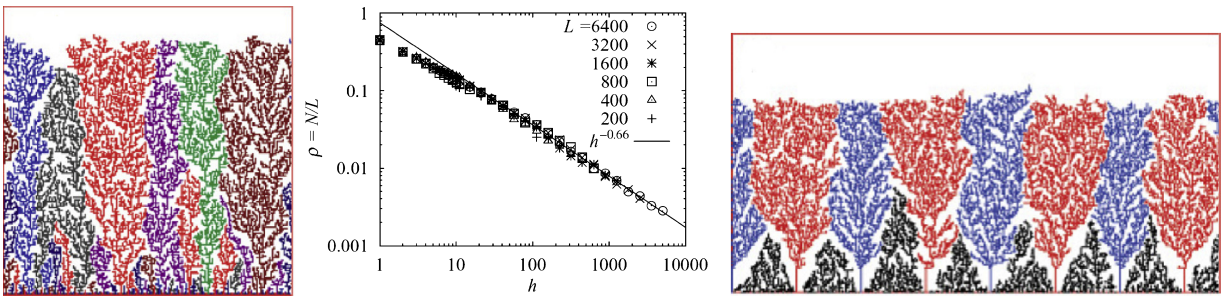

Fig. 6. From [9]. Domain structure in BD aggregate. (a) Domain competition, and (b) domain population density ρ versus height h in a double-logarithmic plot. (c) Domains on a substrate with an array of nanopillars. System sizes are (a) $L \times H = 200^2$, and (c) 400×200.

$$\mathcal{W} = L^{\alpha} f\left(h/L^{z}\right) \tag{17}$$

where $z = \alpha/\beta$ is the dynamical exponent, and $f(x)$ is a scaling function which is constant for $x \gg 1$ and is proportional to x^{β} for small x.

We are interested in domain properties within the BD model [9]. When the first adatom deposited touches on a flat substrate, it freezes to initiate a first domain of an adsorbate crystal. The second adatom may be deposited far from the first one and initiates another crystal domain. Alternatively, it may touch to the first deposited adatom and be incorporated into the first domain. Subsequently deposited adatoms initiate new domains, or are incorporated into an already existing one. The domain of the landing atom is assigned to the domain of the atom below if there is one. Otherwise, it is ascribed to one of the domains in lateral contact with an equal probability.

Many domains extend sideways by capturing adatoms deposited from above, and the neighboring crystal domains compete, as shown in Fig. 6(a). When a domain is completely enveloped from above by neighboring domains, it is cut from the supply of adatoms and stops growing. Through the competition, the domain density decreases as the aggregate grows as a power law

$$\rho \sim h^{-\gamma} \tag{18}$$

as shown in Fig. 6(b). Since the growth front of a BD aggregate has a self-affine property, theory expects that the decrement of the population density of domains ρ as a function of the height h is determined with the dynamical exponent z for the self-affine growth front such that $\gamma = 1/z$. The $(1+1)$-dimensional BD model is known to belong to the universality class of the Kardar–Parisi–Zhang (KPZ) model [24], where the values of exponents are exactly known to be $\alpha = 1/2$, $\beta = 1/3$ and $z = 3/2$. The population density ρ obtained by KMC simulations is found to agree with the theoretical expectation $\gamma = 1/z$, as shown in Fig. 6(b).

When the substrate is patterned with an array of nanopillars, those domains growing on pillar tops have an advantage in capturing deposited adatoms over the domains growing between pillars. When pillars are high or dense, the domains growing on pillar tops envelop those growing between pillars, and the latter are blocked from growing, as shown in Fig. 6(c). Hence, the pillar spacing controls the grain size.

Since a domain growing on top of pillars has only little contact with the substrate at the nucleation center, it should be less affected by the misfit strain between the adsorbate and the substrate. However, the grown BD aggregate contains a lot of vacancies, and its growth front is very rough. These characteristics are far from the actual configuration of adsorbate crystals on patterned substrates [3]. Experiments are performed at a finite temperature, and adatoms can diffuse along the surface of the adsorbate crystal. Lateral diffusion makes adsorbate crystals compact and a growth front smooth. To incorporate surface diffusion in a simple way, we allow those adatoms loosely bonded with only an underlying atom to diffuse laterally at the same height (intralayer diffusion). When diffusing adatoms touch other adatoms laterally, they are in low energy states such that they cannot further migrate thermally. Furthermore, in order to make a growth front flat, adatoms at island edges are allowed to hop down one level (interlayer transport). With these intralayer and interlayer diffusion processes, adsorbate crystals become dense, and domain boundaries are almost vertical, as shown in Fig. 7(a). Though the growth front is almost flat, fluctuation still remain and the domain competition leads to the domain coarsening when starting from a flat substrate. As a function of the height h of deposited material, the domain density is found to decrease as $\rho \sim h^{-1}$.

During deposition on the patterned substrate with nanopillars, domains grown on pillar tops spread sideways quite rapidly, and suppress growth of domains between pillars. Adsorbed crystals have very flat growth fronts and domain boundaries are also straight, as shown in Fig. 7(b). These results are in qualitative agreement with observations made in the experiment [3]. Adatom diffusion makes domains growing on pillar tops stable, and the maximum periodicity of pillars for which stability is observed is larger for the case with adatom diffusion than for the case without it.

Fig. 7. From [9]. Domain structure of BD model with diffusion. (a) On a flat substrate, and (b) on a nanopillar substrate. System sizes are (a) $L \times H = 400^2$, and (b) 400×150.

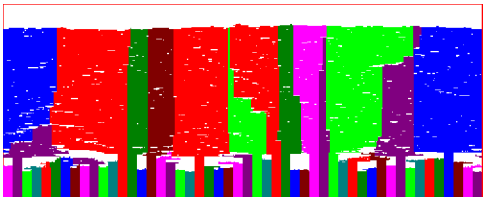

Fig. 8. Domain selection of adsorbate crystals on pillars with random height distribution. Crystals on high pillars survive and compete with neighbors. Further domain coarsening is slow. System size is $L \times H = 500 \times 200$.

6. Summary and discussion

The morphology of a heteroepitaxial overlayer on a nanopatterned substrate surface is studied by kinetic Monte Carlo (KMC) simulations.

We find that islands generically exhibit 3 types of states on nanopatterned substrates: the CB state, the W state, and the imbibition (or CF) state. Hysteresis loops are found between these states. This is similar to the case of liquids. However, since mass transport is controlled by surface diffusion, the dynamics of transition from one state to the other is different from the case of liquids. In addition, crystalline anisotropy can play an important role, especially in the presence of facets.

One important difference between nanogroove and nanopillar arrays is that we expect the collapse transitions to be reversible for nanogrooves, while they should be irreversible for nanopillars, due to the pinning of the triple line. This has been experimentally checked in the case of liquids [25].

In KMC simulations of growth by deposition on a nanopatterned substrate, the CB state is found to be possible, within models with no or reduced island relaxation. Hence it was shown that growth in the CB state can be achieved by shadowing effects in the presence of significant lateral growth of the islands on the pillars. The result may provide hints for GaN heteroepitaxial growth on a low-temperature buffer layer. Crystallite pillars in the buffer layer are densely packed, and their height is not well aligned. When adsorbate molecules are deposited onto the buffer layer at high temperatures, adatoms can diffuse on a surface of growing adsorbate crystals and they grow laterally. In this case, differences in pillar height are crucial for the survival of a crystal domain. On a high pillar the crystal domain has an advantage as compared to the neighboring domains on lower pillars, as shown in Fig. 8. Thus, large domains with high crystalline quality are achieved in heteroepitaxial growth on a buffer layer [1].

Since experimental systems are three-dimensional with two-dimensional substrate surface, KMC simulations should be extended to three dimensions. Tentative results of KMC simulations on domain coarsening for the BD on a flat substrate show the scaling behavior Eq. (18) with $\gamma \approx 2\beta/\alpha$ [26].

In our deposition model we found adsorbate crystal domain only on a single pillar, because each pillar is assumed to define a crystal domain. This assumption is valid in the case where grains from different pillars are all uncorrelated. However, if some grains can merge when they meet, larger crystal domains over multiple pillars are possible. In order to study this point, one has to use off-lattice models with elastic strain taken into account.

Finally, one important remaining issue is to understand the role of the misfit strain on the wetting properties and growth modes on nano-structured substrates. We hope to report along these lines in the near future.

Acknowledgement

Y.S. acknowledges the financial support provided by a Grant-in-Aid for Scientific Research, Grant No. 23540456, from the Japan Society for the Promotion of Science.

References

[1] H. Amano, N. Sawaki, I. Akasaki, Y. Toyota, Appl. Phys. Lett. 48 (1986) 353.
[2] K. Hiramatsu, S. Ito, H. Amano, I. Akasaki, N. Kuwano, T. Sjiraishi, K. Oki, J. Cryst. Growth 115 (1991) 628.
[3] S.D. Hersee, X.Y. Sun, W.X. Wang, M.N. Fairchild, J. Appl. Phys. 97 (2005) 124308.
[4] D. Quéré, Rep. Prog. Phys. 68 (2005) 2495.
[5] A.B.D. Cassie, S. Baxter, Trans. Faraday Soc. 40 (1944) 546.
[6] R.N. Wenzel, Ind. Eng. Chem. 28 (1936) 988.
[7] Olivier Pierre-Louis, Yukio Saito, Europhys. Lett. 86 (2009) 46004.
[8] Koichi Takano, Yukio Saito, Olivier Pierre-Louis, Phys. Rev. B 82 (2010) 075410.
[9] Yukio Saito, Shoko Omura, Phys. Rev. E 84 (2011) 021601.
[10] Phillipe Gaillard, Yukio Saito, Olivier Pierre-Louis, Phys. Rev. Lett. 106 (2011) 195501.
[11] Maxime Ignacio, Olivier Pierre-Louis, Phys. Rev. B 86 (2012) 235410.
[12] D.E. Temkin, in: Crystallization Processes, Consultants Bureau, New York, 1966.
[13] R.H. Swendsen, Phys. Rev. B 15 (1977) 689.
[14] J. De Connick, F. Dunlop, F. Menu, Phys. Rev. E 47 (1993) 1820.
[15] T.P. Schulze, P. Smereka, Phys. Rev. B 86 (2012) 235313.
[16] Olivier Pierre-Louis, Anna Chame, Yukio Saito, Phys. Rev. Lett. 99 (2007) 136101.
[17] Olivier Pierre-Louis, Anna Chame, Yukio Saito, Phys. Rev. Lett. 103 (2009) 195501.
[18] Y. Saito, Surf. Sci. 586 (2005) 83.
[19] J. Tersoff, A.W. Denier van der Gon, R.M. Tromp, Phys. Rev. Lett. 70 (1993) 1143.
[20] J. Bico, C. Tordeux, D. Quéré, Europhys. Lett. 55 (2001) 214.
[21] A. Lafuma, D. Quéré, Nat. Mater. 2 (2003) 457.
[22] R.D. Narhe, D.A. Beysens, Phys. Rev. Lett. 93 (2004) 076103.
[23] F. Family, T. Vicsek, J. Phys. A 18 (1985) L75.
[24] Mehran Kardar, Giorgio Parisi, Yi-Cheng Zhang, Phys. Rev. Lett. 56 (1986) 889.
[25] R.J. Vranken, H. Kusumaatmaja, K. Hermans, A.M. Prenen, O. Pierre-Louis, C.W.M. Bastiaansen, D. Broer, Langmuir 26 (2010) 3335.
[26] K. Osada, H. Katsuno, T. Irisawa, Y. Saito, private communication, 2013.